



## TIPP 2011 - Technology and Instrumentation for Particle Physics 2011

## Development of Ultra-Thin GaAs Photocathodes

Ryan Dowdy<sup>a,1</sup>, Klaus Attenkofer<sup>b</sup>, Henry Frisch<sup>b,c</sup>, Seon Woo Lee<sup>c</sup>, Xiuling Li<sup>a</sup>,  
Steve R. Ross<sup>c</sup> for the Large Area Photodetector Collaboration<sup>2</sup>

<sup>a</sup>Department of Electrical and Computer Engineering, Micro and Nanotechnology Laboratory, University of Illinois at Urbana-Champaign, 208 N. Wright St, Urbana IL 61801, USA

<sup>b</sup>Enrico Fermi Institute, University of Chicago, 5640 S. Ellis Ave., Chicago IL 60637, USA

<sup>c</sup>Argonne National Laboratory, 9700 S. Cass Ave., Argonne, IL 60439, USA

### Abstract

An ultra thin and highly efficient photocathode structure is designed and optimized for the 400nm optical wavelength regime. The cathode thickness is comparable to the mean free path of the photoelectron allowing design concepts which are built on non-thermalized photoelectrons. Designs for ultra-low emittance and high quantum efficiency are proposed and first test structures are grown and characterized. Additionally, a discussion on the specifics of the transfer and bonding process of ultra-thin cathodes is presented.

© 2012 Published by Elsevier B.V. Selection and/or peer review under responsibility of the organizing committee for TIPP 11. Open access under [CC BY-NC-ND license](https://creativecommons.org/licenses/by-nc-nd/4.0/).

**Keywords:** Photocathode; NEA; low emittance; high quantum efficiency; device design; visible light photodetector, non-thermalized, electron momentum, GaAs L-valley, blue photocathode

### 1. Introduction

GaAs based cathodes are widely used for photon detection and as electron sources for accelerator applications. They are typically optimized for the infrared (IR) regime but seldomly used in the blue and ultra violet spectral range. Commercial IR-GaAs transmission photocathodes show very poor quantum efficiency in the 400nm wavelength regime, have relatively high dark current, and are significantly more expensive to produce than standard alkali cathodes, usually used in this wavelength regime.

However, the development of a transmission- GaAs-cathode, optimized for the blue wavelength range is an interesting opportunity to prove the wide wavelength tunability of this material class allowing multi-color response and sensitivity, the feasibility of new device design-concepts with unprecedented high quantum efficiency requiring well defined crystalline materials, and the capability to optimize band structure properties to achieve ultra-low emittance; a property which is of great advantage in high resolution imaging applications.

The purpose of this work is to optimize a device structure with a thickness close to the mean free path length of the photoelectron, avoiding thermalization and randomization[1] of the carrier. Simulation and

<sup>1</sup>Email: [rdowdy2@illinois.edu](mailto:rdowdy2@illinois.edu)

<sup>2</sup> Large Area Picosecond Photodetector Collaboration: <http://psec.uchicago.edu/index.php>

growth tools, typically used in semiconductor device development and production, allow us to optimize complex doping and band gap grading approaches to produce internal electrical fields which break the symmetry of the device, thus forcing the photoelectron towards the cathode surface. Consequently, electrons, originally heading the “wrong way”, can be still collected at the surface and emitted. The initial kinetic energy and gained kinetic energy in the potential gradient of carriers is used to overcome the surface barrier allowing reduction of the required negative electron affinity of the surface, and the dark current of the device.

This paper summarizes our plans and progresses in developing these novel cathodes. It includes the design of the cathode structure, the growth of the materials, the bonding and thinning of the cathode, and the surface modification during the activation process.

## 2. The Design Concepts of Ultra-Thin Photocathodes

Due to the negligible photon-momentum, propagation direction and kinetic energy of the photoelectron solely depend on the photon energy and the details of the band structure of the absorbing material. This effect is widely used for the development of GaAs photocathodes to create spin polarized electrons using spin polarized photons close to the absorption threshold [2]. Our goal is to apply similar design rules for a device structure which conserves the original photoelectron properties produced by a 400nm photon. The key to this approach is the Three-Step-Spicer model [3] predicting that the emission probability of the photoelectron is equal to the product of absorption, transport to the surface, and escape probability. Separation of the three processes allows us to describe the photoelectron properties after each stage of the model and correlate its fate with the structure of the device.

The probability to absorb a photon and the properties of the photoelectron are widely different for the 800nm wavelength typically used for device optimization and the 400nm the wavelength range of interest for this work. An IR-photon ( $\sim 1.5\text{eV}$ ) is absorbed by valence electrons close to the  $\Gamma$ -point, resulting in a vanishing momentum and kinetic energy of the photoelectron. This correlates to a carrier energy of about 1.4eV above the Fermi level expecting that the Fermi level is close to the top of the valence band[4]. According to Fermi's Golden rule, the weak absorption is a direct consequence of the large curvature of the band around the  $\Gamma$ -point and the resulting low density of unoccupied states. The absorption length is in the order of micrometers requiring a cathode of this thickness to achieve maximum absorption.

High energetic photons with wavelength around 400nm (3.1eV) will create photoelectrons which will mostly populate the L-valley. This corresponds to photoelectrons with a relatively well defined kinetic energy of about 0.3eV higher than conduction band electrons at the  $\Gamma$ -point. They mainly propagate along the  $\langle 111 \rangle$  or corresponding crystal direction. The extremely high density of states in comparison to the  $\Gamma$ -point absorption explains the dramatic change of absorption length by nearly three orders of magnitude (20nm-40nm) [5] and consequently an optimum cathode thickness of only 50nm-100nm.

The large difference in absorption cross-section provides an easy way to optimize the cathode for the two wavelength ranges. A thin 50nm-100nm thin cathode will be highly sensitive to 400nm but will only absorb the IR photons with 1% probability. On the other hand, blue photons will be predominantly absorbed in the IR-cathode at the entrance window. Strong scattering mechanisms with a mean free path of about 50nm-100nm, caused by ionized impurity scattering due to high dopant levels of the cathode (about  $10^{18}\text{cm}^{-3}$  Zn-atoms)[6] and defect scattering caused by the bonding of the layer to glass will reduce the quantum efficiency significantly.

Since the thickness of the thin “blue” cathode is comparable to the mean free path of the photoelectron[7], the photocathode can be optimized to preserve the properties of the original photoelectron. This gives interesting possibilities to tailor its emittance and timing properties which cannot be done for thick IR cathodes.

Due to the standard activation process[8, 9], most GaAs photocathodes have a crystal orientation with a GaAs(001) surface with a reconstructed surface which is Ga terminated. As described above, the photoelectron will propagate mainly along the 8 equivalent  $\langle 111 \rangle$  crystal directions. The probability to find a photoelectron on one of the three axes is 1/8 since there is no symmetry break. Four of these axes are penetrating the emission side of the GaAs(001) crystal resulting in a maximal QE of 50%. Each of the  $\langle 111 \rangle$ -axis has a  $45^\circ$  degree angle towards the surface normal resulting in a very large emittance of nearly  $1\pi$ - $2\pi$  sr.

The second interesting opportunity is to create a cathode with reduced emittance. One of the eight predominant propagation directions will be selected by aligning the cathode surface with the propagation direction of the photoelectron, in other words, to use a GaAs (111) crystal. This will significantly reduce the feasible QE to 12.5% (1/8) but will also reduce the emittance in comparison to a GaAs(100) cathode. A quantitative description of the emittance for electrons in the L-valley, like provided for the  $\Gamma$ -electrons[10], is currently not available.

An additional optimization parameter is the introduction of an electric field inside the cathode. This can be done either by gradual variation of the compound from AlAs to GaAs, doping profile[11], or a combination of both. This method is creating a symmetry break which will increase QE and also the emittance.

The last determining step is the emission of the photoelectron from the surface of the cathode. To achieve a high probability for emission the electron affinity has to be negative. A negative electron affinity is produced by creating a dipole layer, composed of a highly p-doped GaAs top layer and a surface layer acting as electron donor (like an n-type impurity), namely a Cs-O sub-monolayer on the surface and the first few layers of the GaAs crystal.

Structures with negative electron affinity were found for the most important surface types, e.g. GaAs (100) [8, 9], GaAs(110) [6], and for GaAs(111) [12]. Experimental and theoretical studies[10] also show that a thin dipole layer of about 20nm thickness will conserve the original photoelectron angle distribution implying a negligible scattering probability of the photoelectron. However, this is in contradiction to previous publications[7] and will need experimental proof.

Using the fact that the carriers are not thermalized and still in the L-valley one can tolerate a reduced negative affinity up to 0.3eV. Detailed studies of the changes of the electron affinity with coverage and surface reconstruction are available [9] which show that the work function variation is within 0.2eV over a wide range of Cs coverage and surface reconstructions. This means that the long-term stability of such a cathode should be much longer than fragile GaAs IR cathodes. We also expect that the increase of the electron affinity will yield a lower dark current.

### 3. Design of Ultra-Thin Photocathodes

Our design goal is a transmission photocathode that operates at 400nm with a peak quantum efficiency larger than 50%. According to the previous discussion an ultra-thin GaAs cathode, e.g. a cathode with a thickness smaller than the mean free path length of the photoelectron, using intrinsic generated momentum/kinetic energy and an integrated electric field should show such a performance. Photocathode emittance can be adjusted via surface crystal orientation and tuning the potential barrier at the surface.

Key to the increased quantum efficiency is the doping profile. It has to provide the necessary conductivity to avoid charging effects for high-count rate applications, reduced ionized impurity scattering to maximize the mean free path length of the photoelectrons, and provide a highly p-doped surface to allow successful activation. Using the Silvaco PISCES/Atlas code for device simulation we

performed various simulations of the expected electric field distribution for various doping profiles.  $p^{++}$ - $p$ - $p^{+}$ -profiles like shown in Figure 1 are fulfilling all necessary conditions.

The thickness of the entrance window has to be minimized to avoid large absorption and increased scattering probability for the produced photoelectrons. However, a too thin layer will increase the risk of dopant diffusion during the activation process and too small conductivity. The proposed layer thickness is 20nm at a doping concentration of  $1 \times 10^{19} \text{ cm}^{-3}$ . This layer will absorb already 36% of the photons and therefore contributes significantly to the total quantum efficiency. The optimization of the lightly doped layer is not only determined by the ratio of absorption- and scattering probability but also by practical reasons like minimizing the risk of damage during the bonding and transfer process, and significant dopant diffusion during the high temperature activation process. A lightly doped region with a thickness of about 60nm is necessary to achieve a total absorption of 83% of the incoming photons (about 47% absorption within the intrinsic layer). To optimize the layer thickness we decided not to perform a Monte Carlo simulation but to grow a set of cathodes with varying intrinsic layer thickness (carrier concentration  $1 \times 10^{17} \text{ cm}^{-3}$ ) since mean free path of electrons with various energetic conditions and doping concentrations are only roughly known. A set with thicknesses with 20nm, 40nm, 60nm, and 80nm was grown.

Similar to the entrance window we decided on a 20nm thick exit window. To allow the activation of the cathode using known recipes we decided to use a dopant concentration of  $1 \times 10^{18} \text{ cm}^{-3}$ . The contribution of carriers produced by photoabsorption in this layer is negligible.

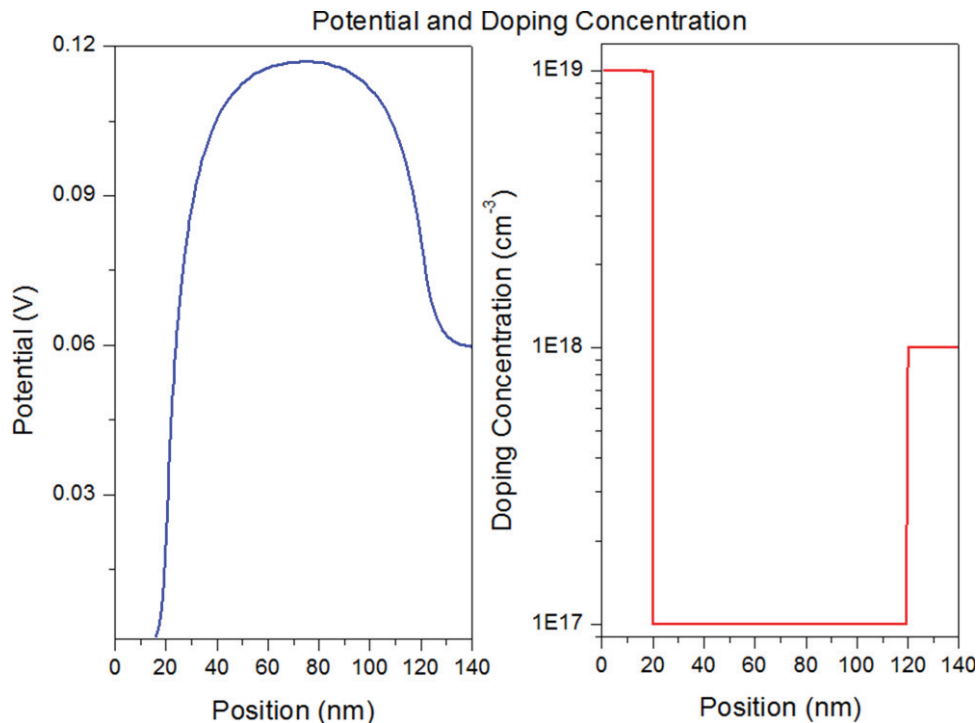


Fig. 1: Simulation of the potential distribution inside a 140nm thick  $p^{++}$ - $p$ - $p^{+}$  cathode structure; the position 0 nm corresponds to the cathode window side and at 140 nm is the emitting surface. The left plot shows the transversal potential distribution, the right plot the corresponding dopant concentration throughout the photocathode.

The cathodes will be activated following a known activation recipe[13]. To test the effect of reduced negative electron affinity we will activate both, a Ga-rich GaAs(001)-(4x2)/c(8x2) as well as an As-rich GaAs(001)-(2x4)/c(2x8) surface. In both cases we will apply a high Cs coverage of 60%-80%; this coverage will result in a reduced electron affinity of about 0.1eV in comparison to the maximal value but have the advantages that a variation of the Cs coverage in the 10% range should have no influence on the cathode functionality. In the case of the As-rich surface we expect a constant electron affinity in the coverage range of 40% to 80%.

To test the device functionality independent from possible effects by the transfer and bonding process we will grow not only transmission cathodes but also comparable films which are separated by a 2 $\mu$ m thick Al<sub>0.75</sub>Ga<sub>0.25</sub>As -buffer layer from the substrate. The layer is p<sup>++</sup> doped to prevent back diffusion of photoelectrons produced in the buffer layer and substrate. This will ensure that we can test the hypothesis of non-thermalized and randomized photoelectrons from ultra thin cathodes without the needs of developing a transfer and bonding technique which does not introduce strain and defects.

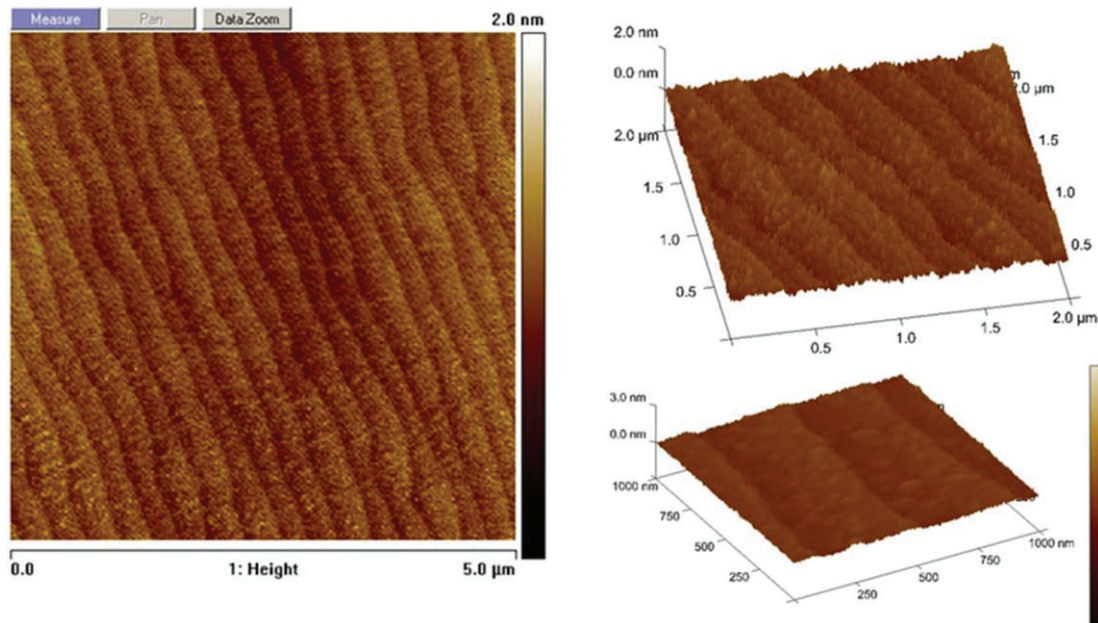


Fig. 2: Atomic Force Microscope image of photocathode surface after atmospheric MOVPE growth. Before transfer and cesiation, the low surface roughness (.3 nm rms) and 300 nm wide terraces indicate atomic smooth terraces.

#### 4. Fabrication of Ultra-Thin Photocathodes

The missing key to create ultra-thin photocathodes lies in the fabrication process. While the silicon industry has long produced bonded thin-film products (SOI)[14], GaAs has not been as fortunate. Without a robust natural oxide, transplanting thin GaAs films was reliant upon intermediate layers consisting of adhesive[15] or polymers. While this is sufficient in low-temperature and atmospheric conditions, it would never survive a photocathode activation and poison the vacuum conditions finally destroying the activation layer. Work has been done to bond GaAs to various materials without the need for adhesives[16, 17]. Recently, InP wafers have been bonded to SiO<sub>2</sub>/Si substrates with the use of SiO<sub>2</sub> as



intermediate layers with impressive results[18]. These methods should be directly applicable to GaAs, to fabricate thin GaAs layers upon a glass substrate which is essential for a transmission photocathode.

### *Growth Method*

Single crystalline GaAs with low defect densities and atomically smooth surface is important to achieve good mean free path length for the photoelectrons and a successful activation resulting in high quantum efficiency. A test structure has been fabricated to characterize material quality. Photocathode fabrication began with GaAs (001) semi-insulating (SI) substrates on which the photocathode was grown. An atmospheric Thomas Swan metalorganic vapor phase epitaxy (MOVPE) system was used to grow subsequent layers. Trimethylgallium (TMGa) and trimethylaluminum (TMAI) were used as the metalorganic group III sources. 10% Arsine ( $\text{AsH}_3$ ) mixture was used as the group V hydride with high-purity hydrogen (palladium diffusion cell) used as the carrier gas. Diethylzinc (DEZn) is used as the p-type doping metalorganic precursor. Carbon has been shown to have adverse effects on photocathode performance[19]. Doping levels were calibrated using a Hall effect measurement system in a van der Pauw configuration[20].

Growth started with a 100 nm intrinsic layer of GaAs buffer directly on the GaAs (100) SI substrate. A 500nm sacrificial layer of  $\text{Al}_{0.75}\text{Ga}_{0.25}\text{As}$  was deposited subsequently. High aluminum content is generally chosen to ensure etching selectivity and reduce etch damage of the photocathode for releasing after the bonding process. The active layers were grown in reverse order as the  $\text{AlGaAs/GaAs}$  heterojunction will eventually become the photocathode surface in the final structure. Next, a thin highly doped layer ( $\sim 10^{18} \text{ cm}^{-3}$ ) was deposited on the surface to create a sharp bend in the conduction band to reduce the surface potential to help achieve NEA. The lightly doped region ( $\sim 10^{17}$ ) was grown next and the final thickness is determined from calibration structures. Finally, regions of Zn doped GaAs, ranging from p to  $p^{++}$  ( $10^{18} \text{ cm}^{-3}$ ), were formed, creating a dopant gradient for the electric field. Figure 2 shows an Atomic Force Microscope image of the material post-growth exhibiting atomic smoothness, with wide terraces indicating uniform epitaxy across the substrate.

During transport and cathode thinning the cathodes are exposed to air which will result in an oxide film on the cathode exit window. This layer will be removed by an etch in an HCl and isopropyl alcohol (HCL-IPA) under inert atmosphere (details are described elsewhere[9]). To compensate for the loss of highly p-doped material we will grow the  $p^{++}$  window a few nanometers thicker. Exact etching conditions, including time and temperature will be determined using calibration structures.

### *Bond & Transfer*

Prior to cesiation of the surface, the transfer of the photocathode must be complete as any exposure to oxygen will spoil NEA layer if bonding is performed subsequently. Transplanting the nanometer scale photocathode involves removing the photocathode from its host substrate and bonding it to a new window substrate (B33 borofloat glass). Cesium of the GaAs surface occurs at UHV pressures ( $\sim 10^{-10}$  Torr) and temperatures in excess of 500 C°. Choice of intermediate bonding layers is important to maintain bond integrity throughout the activation process. Deposition of thin bi-layer of low-stress PECVD  $\text{SiNx/SiO}_2$  ( $\sim 50\text{nm}$  each) is performed before bonding occurs. SiNx is used for an adhesion layer for the GaAs and  $\text{SiO}_2$  provides a strong homogenous bond with the window substrate. The empirical limit of “bondability” between two substrates depends on the surface roughness. An average surface roughness less than 1 nm(rms) should be adequate for a good bond[21]. Preliminary AFM results show a roughness of  $\sim 2 \text{ nm(rms)}$  for the PECVD films, which should be sufficient for bonding. Utilizing

a custom built bonding press that controls bonding pressure and temperature in an atmospheric controlled environment (vacuum or  $N_2$ ) wafer and window are bonded together. Extended bakeouts and surface plasma treatment before bonding can reduce interfacial voids, increasing bond integrity[18].

Post-Bonding, the handle substrate is removed via a series of chemical etches leaving only the photocathode remaining. Using photoresist to protect the sides of the photocathode, citric acid is used to etch away the GaAs bulk substrate which terminates on the AlGaAs sacrificial layer. The AlGaAs sacrificial layer is then removed via a hydrofluoric acid etch (selective against GaAs) which leaves behind an intact photocathode ready for cesiation. The etch process will be performed in inert atmosphere and the sample will be directly transferred under inert atmosphere to the activation UHV chamber.

## 5. Conclusion

Significantly increased optical absorption of GaAs in the short wavelength range allows the design of ultra-thin, highly efficient cathodes with thicknesses comparable to the mean free path length of the photoelectron. This in combination with the strong  $k$ -dependence of the GaAs band structure results in different photoelectron emission properties dependent on the photon energy. The correlation between  $k$ - and real space is used to select the optimum crystal orientation for a given application. It is noticeable that activation procedures, e.g. a surface treatment to achieve negative electron affinity, are documented for most common surfaces allowing a large flexibility in the design.

Based on these considerations, a set of cathode structures optimized for quantum efficiency in the 400nm wavelength regime was proposed, the electric field distribution simulated, and the structure grown. The cathode thickness is varying between 60nm and 120nm, shows a  $\Delta$ -like  $p^{++}$ - $p$ - $p^+$  doping-profile, and has a (001) surface. The proposed cleaning and activation process follows a well-known recipe. The expected quantum efficiency should be larger than 50%.

The  $\Delta$ -like  $p^{++}$ - $p$ - $p^+$  doping-profile will have two major advantages in comparison to conventional cathodes with constant doping. Most photons will be produced inside the lightly doped area of the cathode. The mean free path length is strongly enhanced due to the suppressed ionized impurity scattering within the lightly-doped layer. Additionally, the doping profile creates an internal field which provides an acceleration of the produced photoelectrons towards the cathode surface. The 20nm thin highly  $p$ -doped surface and the Cs/O activation layer should not significantly increase carrier scattering according to literature.

The cathode structure was grown and first characterization measurements performed. The test of the emission and quantum efficiency properties will be first performed on a cathode in reflection geometry even if our final goal is to develop a transmission cathode. The reflection cathode will allow us to test our device structure. In a second step we will approach the challenges to transfer and bond an ultra-thin GaAs film without introducing defects and strain.

## Acknowledgements

Work at Argonne National Laboratory was supported by the U. S. Department of Energy, Office of Science, Office of Basic Energy Sciences and Office of High Energy Physics under contract DE-AC02-06CH11357.

## References

- [1] W. E. Spicer and A. Herrera-Gomez, "Modern theory and applications of photocathodes," *SPIE MILESTONE SERIES MS*, vol. 169, pp. 104–119, 2001.
- [2] D. T. Pierce, R. J. Celotta, G. Wang, x, C, W. N. Unertl, A. Galejs, C. E. Kuyatt, and S. R. Mielczarek, "The GaAs spin polarized electron source," *Review of Scientific Instruments*, vol. 51, pp. 478–499, 1980.
- [3] W. E. Spicer, "Negative affinity 3–5 photocathodes: Their physics and technology," *Applied Physics A: Materials Science & Processing*, vol. 12, pp. 115–130, 1977.
- [4] H. Ehrenreich, "Band Structure and Electron Transport of Gaas," *Physical Review*, vol. 120, pp. 1951–1963, 1960.
- [5] H. C. Casey, D. D. Sell, and K. W. Wecht, "Concentration dependence of the absorption coefficient for n– and p–type GaAs between 1.3 and 1.6 eV," *Journal of Applied Physics*, vol. 46, p. 250, 1975.
- [6] T. Yamada, "STM, STS, and local work function study of Cs/p-GaAs(110)," *Surface Science*, vol. 479, pp. 33–42, 2001.
- [7] B. Yang, G. Ciullo, V. Guidi, and L. Tecchio, "Monte-Carlo Simulation of a Gaas Electron Source," *Journal of Physics D-Applied Physics*, vol. 25, pp. 1834–1837, Dec 14 1992.
- [8] I. M. Vitomirov, A. Raisanen, A. C. Finnefrock, R. E. Viturro, L. J. Brillson, P. D. Kirchner, G. D. Pettit, and J. M. Woodall, "Geometric Ordering, Surface-Chemistry, Band Bending, and Work Function at Decapped Gaas(100) Surfaces," *Physical Review B*, vol. 46, pp. 13293–13302, Nov 15 1992.
- [9] O. E. Tereshchenko, V. L. Alperovich, A. G. Zhuravlev, A. S. Terekhov, and D. Paget, "Cesium-induced surface conversion: From As-rich to Ga-rich GaAs(001) at reduced temperatures," *Physical Review B*, vol. 71, Apr 2005.
- [10] Z. Liu, Y. Sun, P. Pianetta, and R. F. W. Pease, "Narrow cone emission from negative electron affinity photocathodes," *Journal of Vacuum Science & Technology B*, vol. 23, pp. 2758–2762, Nov-Dec 2005.
- [11] B. K. Chang, Y. J. Zhang, Z. Yang, J. Niu, and J. J. Zou, "Distribution of carriers in gradient-doping transmission-mode GaAs photocathodes grown by molecular beam epitaxy," *Chinese Physics B*, vol. 18, pp. 4541–4546, Oct 2009.
- [12] D. C. Rodway and M. B. Allenson, "In situ surface study of the activating layer on GaAs (Cs, O) photocathodes," *Journal of Physics D: Applied Physics*, vol. 19, p. 1353, 1986.
- [13] V. V. Bakin, A. A. Pakhnevich, A. G. Zhuravlev, A. N. Shornikov, I. O. Akhundov, O. E. Tereshechenko, V. L. Alperovich, H. E. Scheibler, and A. S. Terekhov, "Semiconductor surfaces with negative electron affinity," *e-Journal of Surface Science and Nanotechnology*, vol. 5, pp. 80–88, 2007.
- [14] M. Bruel, B. Aspar, and A. J. AubertonHerve, "Smart-cut: A new silicon on insulator material technology based on hydrogen implantation and wafer bonding," *Japanese Journal of Applied Physics Part 1-Regular Papers Short Notes & Review Papers*, vol. 36, pp. 1636–1641, Mar 1997.
- [15] E. Yablonovitch, T. Gmitter, J. P. Harbison, and R. Bhat, "Extreme Selectivity in the Lift-Off of Epitaxial Gaas Films," *Applied Physics Letters*, vol. 51, pp. 2222–2224, Dec 28 1987.
- [16] G. Kastner, T. Akatsu, S. Senz, A. Plossl, and U. Gosele, "Large-area wafer bonding of GaAs using hydrogen and ultrahigh vacuum atmospheres," *Applied Physics a-Materials Science & Processing*, vol. 70, pp. 13–19, Jan 2000.
- [17] J. Schone, F. Dimroth, A. W. Bett, A. Tauzin, C. Jaussaud, and J. C. Roussin, "III-V solar cell growth on wafer-bonded GaAs/Si-substrates," in *Photovoltaic Energy Conversion, Conference Record of the 2006 IEEE 4th World Conference on*, 2006, pp. 776–779.
- [18] D. Liang, A. W. Fang, H. Park, T. E. Reynolds, K. Warner, D. C. Oakley, and J. E. Bowers, "Low-Temperature, Strong SiO<sub>2</sub>-SiO<sub>2</sub> Covalent Wafer Bonding for III–V Compound Semiconductors-to-Silicon Photonic Integrated Circuits," *Journal of Electronic Materials*, vol. 37, pp. 1552–1559, 2008.
- [19] R. L. Bell, *Negative electron affinity devices*: Clarendon Press, Oxford, 1973.
- [20] L. J. van der Pauw, "A method of measuring specific resistivity and Hall effect of discs of arbitrary shape," *Phillips Research Reports*, vol. 13, pp. 1–9, 1958.



- [21] C. Gui, M. Elwenspoek, N. Tas, and J. G. E. Gardeniers, "The effect of surface roughness on direct wafer bonding," *Journal of Applied Physics*, vol. 85, pp. 7448-7454, May 15 1999.